DMD Fast Forward. Published on April 14, 2014 as doi:10.1124/dmd.114.058206

Title page

Metabolic activation of the antibacterial agent, triclocarban, by cytochrome P450 1A1 yielding glutathione adducts

Nils Helge Schebb, Jaya B Muvvala, Dexter Morin, Alan R. Buckpitt, Bruce D. Hammock

and Robert H. Rice

Institute of Food Toxicology and Chemical Analysis, University of Veterinary Medicine, University of Hannover, Hanover Germany (NHS)

Department of Molecular Biosciences (JBM, DM, ARB), School of Veterinary Medicine

Department of Entomology and Comprehensive Cancer Center (BDH) and Environmental Toxicology, College of Agricultural and Environmental Sciences (RHR)

University of California

Davis, CA 95616

DMD Fast Forward. Published on April 14, 2014 as DOI: 10.1124/dmd.114.058206
This article has not been copyedited and formatted. The final version may differ from this version.

Running title page

Running Title: GSH conjugates of the antimicrobial agent, triclocarban

Corresponding author:
Nils Helge Schebb
Institute for Food Toxicology and Chemical Analysis
University of Veterinary Medicine
Bischofsholer Damm 15
Hanover, Germany
Email: schebb@wwu.de
Phone: +49 511 856 7780
Fax: +49 511856 7409

Number of text pages: 10
Number of tables: 0
Number of figures: 4
Number of references: 21

Number of words in:
Abstract 199
Introduction 564
Results and Discussion 1497

List of non-standard abbreviations:

ACN	acetonitrile
ESI-MS	electrospray ionization mass spectrometry
GSH	glutathione
m/z	mass to charge ratio
LC	liquid chromatography
P450	cytochrome P450
TCC	3,4,4'-trichlorocarbanilide, triclocarban

Abstract:

Triclocarban (3,4,4'-trichlorocarbanilide; TCC) is an antibacterial agent used in personal care products such as bar soaps. Small amounts of chemical are absorbed through the epidermis. Recent studies show that residues of reactive TCC metabolites are bound covalently to proteins in incubations with keratinocytes, raising concerns about the potential toxicity of this antimicrobial agent. To obtain additional information on metabolic activation of TCC, this study characterized the reactive metabolites trapped as glutathione conjugates. Incubations were carried out with ^{14}C-labeled TCC, recombinant CYP1A1 or CYP1B1 coexpressed with P450 reductase, GSH, glutathione S-transferases and an NADPH generating system. Incubations containing CYP1A1, but not 1B1, led to formation of a single TCC-GSH adduct with a conversion rate of 1% of parent compound in 2 hr. Using high resolution mass spectrometry and diagnostic fragmentation, the adduct was tentatively identified as 3,4-dichloro-3'-glutathionyl-4'-hydroxycarbanilide. These findings support the hypothesis that TCC is activated by oxidative dehalogenation and oxidation to a quinone imine. Incubations of TCDD-induced keratinocytes with ^{14}C-TCC yielded a minor radioactive peak coeluting with TCC-GSH. Thus, we conclude that covalent protein modification by TCC in TCDD-induced human keratinocyte incubations is mainly caused by activation of TCC by CYP1A1 via a dehalogenated TCC derivative as reactive species.

DMD Fast Forward. Published on April 14, 2014 as DOI: 10.1124/dmd.114.058206
This article has not been copyedited and formatted. The final version may differ from this version.

Introduction:

Triclocarban (TCC) is an antimicrobial agent in widespread use in personal care products, particularly in bar soaps, with annual production totaling several million pounds (Halden and Paull, 2005). Due to its lipophilicity, TCC bio-concentrates in the aquatic environment and is one of the most abundant anthropogenic compounds found in sewage sludge (Langford et al., 2011). Moreover, significant TCC bioconcentration in aquatic organisms such as algae, snails (Coogan et al., 2007; Coogan and La Point, 2008) and fish (Schebb et al., 2011a) has been reported.

Despite initial reports that TCC is biologically inactive, more recent work suggests that this chemical may not be as innocuous as once thought. First, TCC may have the potential to act as an endocrine disruptor by enhancing the action of testosterone (Ahn et al., 2008; Chen et al., 2008). While the endocrine disrupting effects were observed only at very high concentrations, TCC inhibits the enzyme, soluble epoxide hydrolase (sEH), with an *in vitro* potency in the low nanomolar range (IC_{50} 13nM) (Morisseau et al., 2009). The effects of TCC on sEH are comparable to activities observed with synthetic inhibitors (?), which have been shown to alter the biological regulation of inflammation, pain and blood pressure *in vivo* (Imig and Hammock, 2009; Inceoglu et al., 2011).

Bathing with TCC-containing soaps typically results in deposition of TCC on human skin of ≈0.3 μg/cm^2(North-Root et al., 1984). A small portion traverses the epidermal barrier and becomes systemically available. Showering with antibacterial soap results in the absorption of ≈0.6% of the applied amount of TCC (Schebb et al., 2011b). Several studies have shown that TCC is extensively metabolized in fish, rodents, monkeys, and humans leading to several phase I and phase II metabolites (Baumann et al., 2010; Schebb et al., 2012b).

Cytochrome P450 enzymes (CYP) play a key role in TCC metabolism. The main phase 1 metabolites in all species are monohydroxylated-TCC derivatives bearing the hydroxyl group *ortho* to the aniline group, namely 2'-OH-TCC and 6'-OH-TCC (Birch et al., 1978; Schebb et al., 2012b, (Baumann et al., 2010). In addition, hydroxylation in the *meta* position (3'-OH-TCC) and substitution of a chlorine atom by a hydroxyl group occurs yielding 3,4-dichloro-4'-hydroxyl carbanilide (DHC) (for the structures of metabolites see (Schebb et al., 2011a). All hydroxylated metabolites undergo extensive phase II conjugation by UDP-glucuronosyl transferases (Schebb et al., 2012b). Further oxidation of 2'OH-TCC, 6'OH-TCC and DHC can generate reactive

DMD Fast Forward. Published on April 14, 2014 as DOI: 10.1124/dmd.114.058206
This article has not been copyedited and formatted. The final version may differ from this version.

quinone imines which can covalently bind to glutathione and small proteins as shown in an electrochemistry liquid chromatography mass spectrometry (EC-LC-MS) approach to mimic formation of reactive metabolites (Baumann et al., 2010). Incubation of spontaneously immortalized keratinocytes with ^{14}C-TCC resulted in small quantities of radioactivity bound covalently to cellular macromolecules (Schebb et al., 2012a). In these experiments adduct formation and oxidative metabolism of TCC was greatly enhanced by pre-incubation with Ah receptor agonist, TCDD, indicating a role for inducible CYP in reactive metabolite formation in keratinocytes. Much previous work has shown that keratinocytes in the skin and in culture express only traces of CYP activity without induction of CYP1A1 and 1B1 using Ah receptor ligands such as TCDD or polycyclic aromatic hydrocarbons (Gotz et al., 2012). The present studies demonstrate the conversion of TCC by CYP1A1 to a reactive metabolite trapped as a glutathione conjugate. Conversion rates were monitored by LC/radioprofiling of extracts of incubations containing ^{14}C-TCC, and the GSH conjugate was characterized by high resolution mass spectrometry.

Materials and Methods:

Radiochemical: ^{14}C-(3,4,4'-Trichlorocarbanilide), uniformly labeled in the chlorophenyl ring, was obtained from Moravek Radiochemicals, Brea, CA at a specific activity of 30 Ci/mole. The material was tested for chemical and radiochemical purity by reverse phase LC and found to be >99.5% pure.

Incubations with recombinant CYP1A1 and CYP1B: Supersomes containing human CYP1A1 or CYP1B1 plus P450 reductase expressed in baculovirus infected insect cells were obtained from BD Biosciences San Jose, CA. Supersomes (500 pmoles P450) were incubated with NADPH generating solution (0.14 mM NADP, 3.8 mM glucose 6-phosphate, 0.1 U glucose-6-phosphate dehydrogenase, 10 mM $MgCl_2$), ^{14}C-TCC (66 DPM/pmol, for metabolite profiling) or unlabeled TCC (for LC-ESI-MS/MS analysis) (10 μM final concentration, added in DMSO to less than 0.1% of the total volume), glutathione (5 mM final concentration) and affinity purified mouse glutathione S-transferases (5 CDNB units/ml). Reactions were carried out in a shaking incubator at 37^o C for 2 hr with a second addition of NADPH generating system at 1

DMD Fast Forward. Published on April 14, 2014 as DOI: 10.1124/dmd.114.058206
This article has not been copyedited and formatted. The final version may differ from this version.

hr. Acetonitrile (3 vol, 4^{o} C) was added to stop the reaction, precipitated protein was removed by centrifugation and the supernatant was lyophilized to dryness.

Keratinocyte culture: Human epidermal spontaneously immortalized keratinocytes (SIK) were cultured with 3T3 feeder layer support in a Dulbecco-Vogt modified Eagle's medium (DMEM)–Ham's F-12 mixture (2:1)(Rea et al., 2006). Newly confluent cultures in 4 ml of medium were incubated in the presence of 10 nM TCDD for 6 hr before addition of 2 μM ^{14}C-TCC (66 DPM/pmol). After incubation for an additional 18 hr, the cells and medium were transferred to centrifuge tubes and mixed with 12 ml of acetonitrile (ACN) and frozen. Samples were centrifuged to remove precipitated protein and the supernatant was lyophilized.

Solid phase extraction: Waters Oasis HLB solid phase extraction columns (500 mg/12 ml extraction cartridge) were prepared by washing with 5 ml of 100% ACN followed by 3 x 5 ml washes with 0.5% formic acid in water. The lyophilized sample was dissolved in 5 ml of 0.5% formic acid and applied to the column. The column was rinsed with 5 x 5 ml of 0.5% formic acid, and TCC metabolites were eluted with 15 ml of 75% ACN - 0.5% formic acid in water. The collected eluate was evaporated to dryness on a centrifugal evaporator under reduced pressure, and the residue was redissolved in 50% ACN - 0.1% formic acid in water for HPLC analysis.

HPLC radioprofiling and LC-MS/MS analysis: Samples were injected onto a Phenomenex-Kinetex XB-C_{18} column (2.6 μm particle size). For radioprofiling, the dimensions of the column were 150 x 4.6 mm, and a solvent flow rate of 1 ml/min was used. A 150 x 2.1 mm column of the same type was eluted at 210 μl/min for LC-ESI-MS/MS analysis. Solvent A was 0.1% formic acid in water and solvent B was 0.1% formic acid - 50% acetonitrile in water. The analytes were eluted by the following gradient: 0-100 min linear from 5% to 100% solvent B, 100-130 min isocratic 100% B. For radioprofiling, fractions were collected at 30 sec intervals and were counted for 2 min in a liquid scintillation counter.

ESI-MS/MS analysis was performed on an Orbitrap XL spectrometer. The analytes were ionized by electrospray ionization with mass resolution set to 15,000. Fragmentation was carried out on the two most abundant ions with collision energy of 35 V. To prevent contamination of the ion source, the first 5 min of the separation were directed to waste. The data were analyzed for GSH adducts utilizing product ion scans and neutral loss scans with Xcalibur Software Version 2.07. For isotope pattern analysis and mass defect filtering, the data were transferred in the cdf format and evaluated with Bruker Data Analysis 4.0 (Bremen, Germany). The settings

were: Isotope pattern of three chlorine containing substances: Delta mass 3.9941±0.05 Da with an abundance of 10% and 30% of the monoisotopic ^{35}Cl analog to screen for molecules containing two and three chlorine atoms, respectively. Mass defect filtering was carried out with Metworks 1.3 (Thermo). The data were analyzed for molecules showing the mass defect of TCC (0.0220±0.05 Da). The range of ±0.05 Da covers most metabolic reactions, but the loss of chlorine or addition of GSH causes a greater increase in mass defect (Zhang et al., 2003; Zhu et al., 2006). Therefore, other filters were used for the mass defects of 2´-OH-TCC GSH adduct -0.0411 Da (Baumann et al., 2010) and potential bis-GSH adduct -0.1093 Da, as well as DHC (-0.0119) and its GSH and bis-GSH adducts -0.0801 Da and -0.1482 Da each in a range of ±0.05 Da.

Results and Discussion

The conversion of TCC to oxidative metabolites and GSH adducts was analyzed by LC-ESI-MS analysis. As shown in Figure 1A,B the total ion current (TIC) using negative ESI of an extract from an incubation containing recombinant CYP1A1 showed two major peaks at 30 and 55 min followed by various signals eluting at the end of the chromatogram. Following positive ionization several additional peaks were detected, while corresponding peaks a and b were still clearly detectable (Supplemental Figure 1). The ESI(-) MS signal obtained with extracts of incubations containing recombinant CYP1B1 displayed a single peak eluting ≈30 min, similar to peak a recovered from incubations containing recombinant CYP1A1. Since the GSH adducts appear to be generated slowly, thereby yielding very small TIC signals, the MS scan data were analyzed for diagnostic fragmentation of GSH adducts, i.e. formation of a fragment at *m/z* 272 in negative ESI and neutral loss of 129 Da in positive ionization mode (Dieckhaus et al., 2005; Ma and Subramanian, 2006). As shown in Figure 2 both analyses showed a single signal at the retention time of peak b indicating that a GSH adduct elutes ≈55 minutes. No peaks were found in the analysis of extracts of incubations containing CYP1B1.

In a complementary strategy, the high resolution MS chromatograms of extracts of CYP1A1 incubations were analyzed for TCC metabolites. With three chlorine atoms, TCC and its metabolites show both a distinct isotopic pattern as well as a high mass defect allowing a specific analysis for unknown metabolites. However, no signals for metabolites bearing three chlorine atoms were found. Since TCC can be oxidatively dehalogenated to DHC (Baumann et

DMD Fast Forward. Published on April 14, 2014 as DOI: 10.1124/dmd.114.058206
This article has not been copyedited and formatted. The final version may differ from this version.

al., 2010), the same analysis was carried out for the isotopic pattern of molecules containing two chlorine atoms. Here a peak eluting at 55 min resulted from the incubation with CYP1A1 (Figure 2C) suggesting that this metabolite has two chlorines. Similarly, mass defect filtering for the GSH-adduct of DHC shows a clear signal at 55 min (Figure 2D), while no further signals could be found for the mass defect of the TCC-GSH adduct. Analyses of extracts prepared from incubations containing CYP1B1 failed to reveal signals consistent with the formation of TCC GSH adducts.

The MS spectra of peak b showed dominant ions at *m/z* 600.0723 in negative ESI mode, with the characteristic pattern of a single charged ion of a compound bearing two chlorine atoms (Figure 1, Figure S1). These are likely the $[M-H]^-$ ions of a TCC metabolite since, in positive ESI, corresponding ions at 2.000 Da higher mass were found (Supplemental Figure 1). The exact (monoisotopic) mass of this metabolite is 601.0801 amu, which corresponds exactly to the calculated mass of a DHC-GSH adduct. Moreover, the observed fragmentation pattern is consistent with the suggested structure of a DHC-GSH adduct. As shown in Figure 4, fragmentation in negative ion mode leads to four major fragments, while positive ESI gave rise to two major fragments. The main fragment at *m/z* 413.1130 amu can be attributed to scission of the carbon nitrogen bond (*a* in Figure 4) of the urea leading to an aniline fragment. This is a major route of fragmentation of TCC and its derivatives following negative ESI (Baumann et al., 2010). The other fragment ions can be assigned to the fragmentation of GSH. Accordingly, the ions at *m/z* 326.9796 and *m/z* 272.0887 are both sides of the product resulting from fragmentation of the carbon thiol bond of GSH (Figure 4*b*, Supplemental Figure 2). The signal at 254.0784 results from further fragmentation at site c. Fragmentation of the amide bonds of GSH yielded fragments at *m/z* 473.0442 and 527.05.44. All major fragments support the suggested structure of the DHC-GSH adduct. Moreover the exact mass of the parent molecule as well as product ions are fully consistent with the calculated masses of the fragments (Figure 4).

The DHC-GSH conjugate can be formed from TCC by dehalogenation and hydroxylation followed by nucleophilic addition to the monochloraniline ring. To support the assumption that the GSH adduct arises via the intermediate formation of DHC, incubation of CYP1A1 with DHC as precursor was carried out. This incubation yielded a peak at the same retention time showing the same ESI-MS, ESI-MS/MS ions as the incubation of TCC (Supplemental Figure 3). Thus, TCC is metabolically activated by oxidative dehalogenation at the monochloraniline ring

DMD Fast Forward. Published on April 14, 2014 as DOI: 10.1124/dmd.114.058206
This article has not been copyedited and formatted. The final version may differ from this version.

and hydroxylation to a *p*-quinone imine which generates the glutathione adduct. Incubation of TCC with CYP1A1 but not 1B1 gave rise to GSH adducts (Figure 1). To obtain quantitative information of GSH adduct formation, incubations were repeated using ^{14}C-TCC with radioprofiling. Incubations containing CYP1A1 gave rise to a peak in the radiochromatogram with a retention time corresponding to peak b (55 min) containing 500 pmol product equivalent to 1% of the initial TCC amount (Figure 1). No radioactive peak was observed in the retention time window for CYP1B1 incubations. In both CYP1A1 and CYP1B1 incubations, a smaller peak eluted from the column at 31 min with a maximum radioactivity of ~1500 DPM (0.3% of the added radioactivity). No structural information could be obtained on this peak due to the small amounts present (Figure 1). Dominant ions using negative ESI observed in extracts from both CYP1A1 and CYP1B1 incubations included those at *m/z* 413, 497, 565, and 597 which revealed neither a chlorine isotope pattern, nor typical GSH fragments (data not shown).

A 2 hr incubation with 0.5 nmol of CYP1A1 led to the formation of 0.5 nmol GSH adduct, or product formation as low as 1 nmol/nmol P450/2 hr. It is difficult to extrapolate from the observed formation rate *in vitro* to the generation of metabolites in tissues *in vivo*. TCC conversion to both oxidative metabolites and *N*-glucuronides is substantially underpredicted by *in vitro* microsomal incubations (Baumann et al., 2010; Schebb et al., 2012b). This low predictability is likely related to the poor water solubility of the compound (142 nM, Snyder et al., 2010), causing a low effective concentration in the assays. Thus, TCC activation might occur to a much greater extent *in vivo*. In fact, the suggested precursor of the reactive metabolite has been found in a number of different organisms ranging from medaka fish to human keratinocytes (Schebb et al., 2011a; Schebb et al., 2012a).

The finding that the TCC-GSH adduct – and thus reactive metabolite - formation is catalyzed by CYP1A1 is consistent with data showing that TCC-protein adduct formation in keratinocytes is increased substantially following induction with TCCD. As shown in Figure 5, incubation of ^{14}C-TCC with TCDD-induced keratinocytes resulted in the formation of multiple polar radiolabeled metabolites resolved by HPLC (a-f). The peaks b, c, d, e, f co-eluted with known TCC metabolites including DHC (b), 2-O-Gluc TCC (c), 3'OH-TCC (d), 2' OH-TCC and 6 OH-TCC (e) and TCC (f). In addition the small peak (a) was tentatively identified as DHC-GSH based on its retention time between 55-58 min. Although this peak represents only a small portion of the metabolites generated (about 1% of the amount of TCC added to the cells) it is

DMD Fast Forward. Published on April 14, 2014 as DOI: 10.1124/dmd.114.058206
This article has not been copyedited and formatted. The final version may differ from this version.

qualitatively and quantitatively consistent with the formation of small amounts of protein bound metabolite and demonstrates the ability of keratinocytes to inactivate the electrophile through conjugation with GSH.

In conclusion, our study supports the hypothesis that TCC can be oxidatively converted to reactive metabolites (Baumann et al., 2010; Schebb et al., 2012a). The GSH adduct formed by CYP1A1 was tentatively identified as 3,4-dichloro-3'-glutathionyl-4'-hydroxycarbanilide, a metabolite which is likely formed via an initial substitution of an aromatic chlorine atom by a hydroxyl group. This is not a common P450 catalyzed reaction but has been reported for certain halogenated aromatics (for review see (Guengerich, 2001). The resulting metabolite, DHC, can be further oxidized to a *p*-quinone imine which is a well-established electrophilic intermediate generated during the activation of several drugs including acetaminophen. Activation of TCC by CYP1A1 to glutathione reactive intermediates is consistent with the large increases in protein adduct observed in TCCD-induced compared to control keratinocyte incubations (Schebb et al., 2012a).

The biological consequences of reactive metabolite formation from TCC cannot be assessed with certainty, but the slow rates of metabolism to both protein- and glutathione-reactive intermediates would suggest minor if any untoward effects. One concern is whether these reactive metabolites bind to nucleophilic sites on DNA. The quinone imine intermediates generated from TCC are soft Lewis acids and would be less likely to react with the hard nucleophilic sites (strong Lewis bases) on DNA bases. A preliminary mutagenicity study of TCC in TCDD-induced keratinocytes showed no detectable mutagenic activity (Supplemental Table 1), a finding consistent with the characteristics of the electrophiles trapped as glutathione conjugates.

Overall, the formation of reactive metabolites, particularly at the levels described here does not translate to a high level of concern for adverse health effects for use of TCC in personal care products. Given the high production volume of TCC and the widespread human exposure, it is surprising that reactive metabolites and GSH adducts of this chemical have not been detected in the last 50 years of use of the compound.

Acknowledgments
We thank Dr. William Jewell for help with LC-MS measurements and Qin Qin for performing mutagenicity assays.

Author contributions

Participated in research design: Schebb, Muvvala, Morin, Buckpitt, Hammock, Rice
Conducted experiments: Schebb, Muvvala, Morin, Rice
Contributed new reagents or analytical tools: Schebb, Hammock
Performed data analysis: Schebb, Muvvala, Morin, Rice
Wrote or contributed to the writing of the manuscript: Schebb, Muvvala, Morin, Buckpitt, Rice

DMD Fast Forward. Published on April 14, 2014 as DOI: 10.1124/dmd.114.058206
This article has not been copyedited and formatted. The final version may differ from this version.

References

Ahn KC, Zhao B, Chen J, Cherednichenko G, Sanmarti E, Denison MS, Lasley B, Pessah IN, Kultz D, Chang DP, Gee SJ, and Hammock BD (2008) In vitro biologic activities of the antimicrobials triclocarban, its analogs, and triclosan in bioassay screens: receptor-based bioassay screens. *Environ Health Perspect* **116:**1203-1210.

Baumann A, Lohmann W, Rose T, Ahn KC, Hammock BD, Karst U, and Schebb NH (2010) Electrochemistry-mass spectrometry unveils the formation of reactive triclocarban metabolites. *Drug Metab Dispos* **38:**2130-2138.

Chen J, Ahn KC, Gee NA, Ahmed MI, Duleba AJ, Zhao L, Gee SJ, Hammock BD, and Lasley BL (2008) Triclocarban enhances testosterone action: a new type of endocrine disruptor? *Endocrinology* **149:**1173-1179.

Coogan MA, Edziyie RE, La Point TW, and Venables BJ (2007) Algal bioaccumulation of triclocarban, triclosan, and methyl-triclosan in a North Texas wastewater treatment plant receiving stream. *Chemosphere* **67:**1911-1918.

Coogan MA and La Point TW (2008) Snail bioaccumulation of triclocarban, triclosan, and methyltriclosan in a North Texas, USA, stream affected by wastewater treatment plant runoff. *Environ Toxicol Chem* **27:**1788-1793.

Dieckhaus CM, Fernandez-Metzler CL, King R, Krolikowski PH, and Baillie TA (2005) Negative ion tandem mass spectrometry for the detection of glutathione conjugates. *Chem Res Toxicol* **18:**630-638.

Gotz C, Pfeiffer R, Tigges J, Ruwiedel K, Hubenthal U, Merk HF, Krutmann J, Edwards RJ, Abel J, Pease C, Goebel C, Hewitt N, and Fritsche E (2012) Xenobiotic metabolism capacities of human skin in comparison with a 3D-epidermis model and keratinocyte-based cell culture as in vitro alternatives for chemical testing: phase II enzymes. *Exp Dermatol* **21:**364-369.

Guengerich FP (2001) Common and uncommon cytochrome P450 reactions related to metabolism and chemical toxicity. *Chem Res Toxicol* **14:**611-650.

Halden RU and Paull DH (2005) Co-occurrence of triclocarban and triclosan in U.S. water resources. *Environ Sci Technol* **39:**1420-1426.

Imig JD and Hammock BD (2009) Soluble epoxide hydrolase as a therapeutic target for cardiovascular diseases. *Nat Rev Drug Discov* **8:**794-805.

Inceoglu B, Wagner K, Schebb NH, Morisseau C, Jinks SL, Ulu A, Hegedus C, Rose T, Brosnan R, and Hammock BD (2011) Analgesia mediated by soluble epoxide hydrolase inhibitors is dependent on cAMP. *Proc Natl Acad Sci U S A* **108:**5093-5097.

Langford KH, Reid M, and Thomas KV (2011) Multi-residue screening of prioritised human pharmaceuticals, illicit drugs and bactericides in sediments and sludge. *J Environ Monit* **13:**2284-2291.

Ma S and Subramanian R (2006) Detecting and characterizing reactive metabolites by liquid chromatography/tandem mass spectrometry. *J Mass Spectrom* **41:**1121-1139.

Morisseau C, Merzlikin O, Lin A, He G, Feng W, Padilla I, Denison MS, Pessah IN, and Hammock BD (2009) Toxicology in the fast lane: application of high-throughput bioassays to detect modulation of key enzymes and receptors. *Environ Health Perspect* **117:**1867-1872.

North-Root H, Demetrulias J, Wester R, Maibach H, and Corbin N (1984) Deposition of 3,4,4'-trichlorocarbanilide on human skin. *Toxicol Lett* **22:**235-239.

Rea MA, Zhou L, Qin Q, Barrandon Y, Easley KW, Gungner SF, Phillips MA, Holland WS, Gumerlock PH, Rocke DM, and Rice RH (2006) Spontaneous immortalization of human epidermal cells with naturally elevated telomerase. *J Invest Dermatol* **126:**2507-2515.

Schebb NH, Buchholz BA, Hammock BD, and Rice RH (2012a) Metabolism of the antibacterial triclocarban by human epidermal keratinocytes to yield protein adducts. *J Biochem Mol Toxicol* **26:**230-234.

Schebb NH, Flores I, Kurobe T, Franze B, Ranganathan A, Hammock BD, and Teh SJ (2011a) Bioconcentration, metabolism and excretion of triclocarban in larval Qurt medaka (Oryzias latipes). *Aquat Toxicol* **105:**448-454.

Schebb NH, Franze B, Maul R, Ranganathan A, and Hammock BD (2012b) In vitro glucuronidation of the antibacterial triclocarban and its oxidative metabolites. *Drug Metab Dispos* **40:**25-31.

Schebb NH, Inceoglu B, Ahn KC, Morisseau C, Gee SJ, and Hammock BD (2011b) Investigation of human exposure to triclocarban after showering and preliminary evaluation of its biological effects. *Environ Sci Technol* **45:**3109-3115.

Snyder EH, O'Connor GA, and McAvoy DC (2010) Measured physicochemical characteristics and biosolids-borne concentrations of the antimicrobial Triclocarban (TCC). *The Science of the Total Environment* **408:**2667-2673

Legends for figures

Figure 1 Radioactivity profile of LC fractions and LC-ESI-(-)-MS chromatograms of incubation of TCC with CYP1A1 (A) and CYP1B1 (B). Insert MS spectrum of the peak eluting at 55.3 min.

Figure 2 Extracted ion signals for diagnostic fragments of GSH adducts of incubation of TCC with CYP1A1. A ESI(-)-MS/MS of the GSH fragment at m/z 227 and B ESI(+)-MS/MS neutral loss scan of 129 Da C Isotopic pattern analysis for two chlorine atomes D Mass defect analysis for the DHC-GSH adduct

Figure 3 Fragmentation pattern of TCC-GSH adduct: A Suggested structure of the adduct dashed lines depict suggested sites of fragmentation (a-f). Adjacent numbers are the *m/z* ratio of the resulting fragments. B: ESI(-)-MS/MS fragment spectra of the ion at m/z 600.07 and C: ESI(+) fragment spectra of TCC-GSH adduct

Figure 4 Radioactivity profile of LC fractions after incubation of TCCD induced kerationcytes with TCC for 24 h hours. The peaks corresponds to DHC-GSH adduct (a), DHC (b), 2-O-Gluc TCC (c), 3'OH-TCC (D), 2' OH-TCC and 6 OH-TCC and TCC (f).

Fig. 1

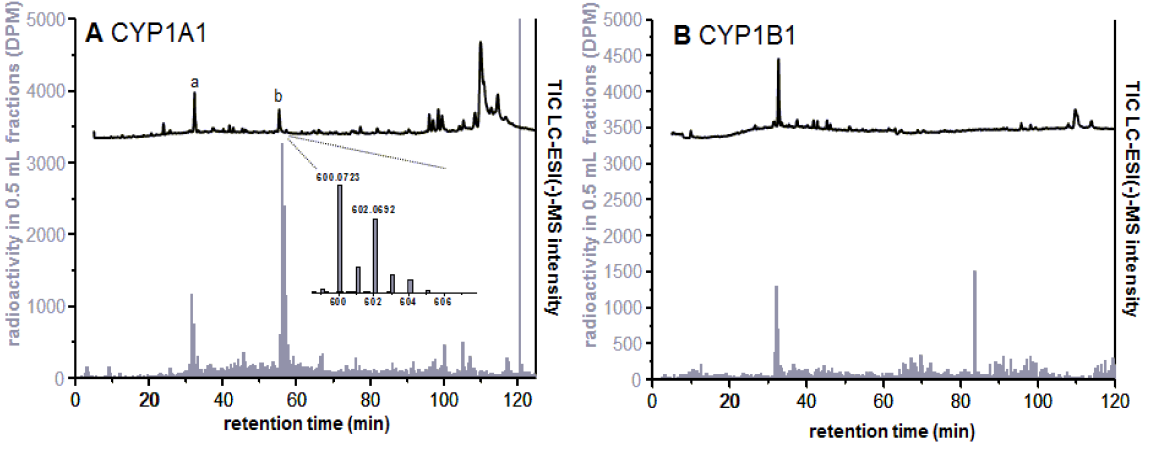
A CYP1A1
a
b
600.0723
602.0692
600
602
604
606
radioactivity in 0.5 mL fractions (DPM)
TIC LC-ESI(-)-MS intensity
retention time (min)
B CYP1B1
radioactivity in 0.5 mL fractions (DPM)
TIC LC-ESI(-)-MS intensity
retention time (min)

Fig. 2

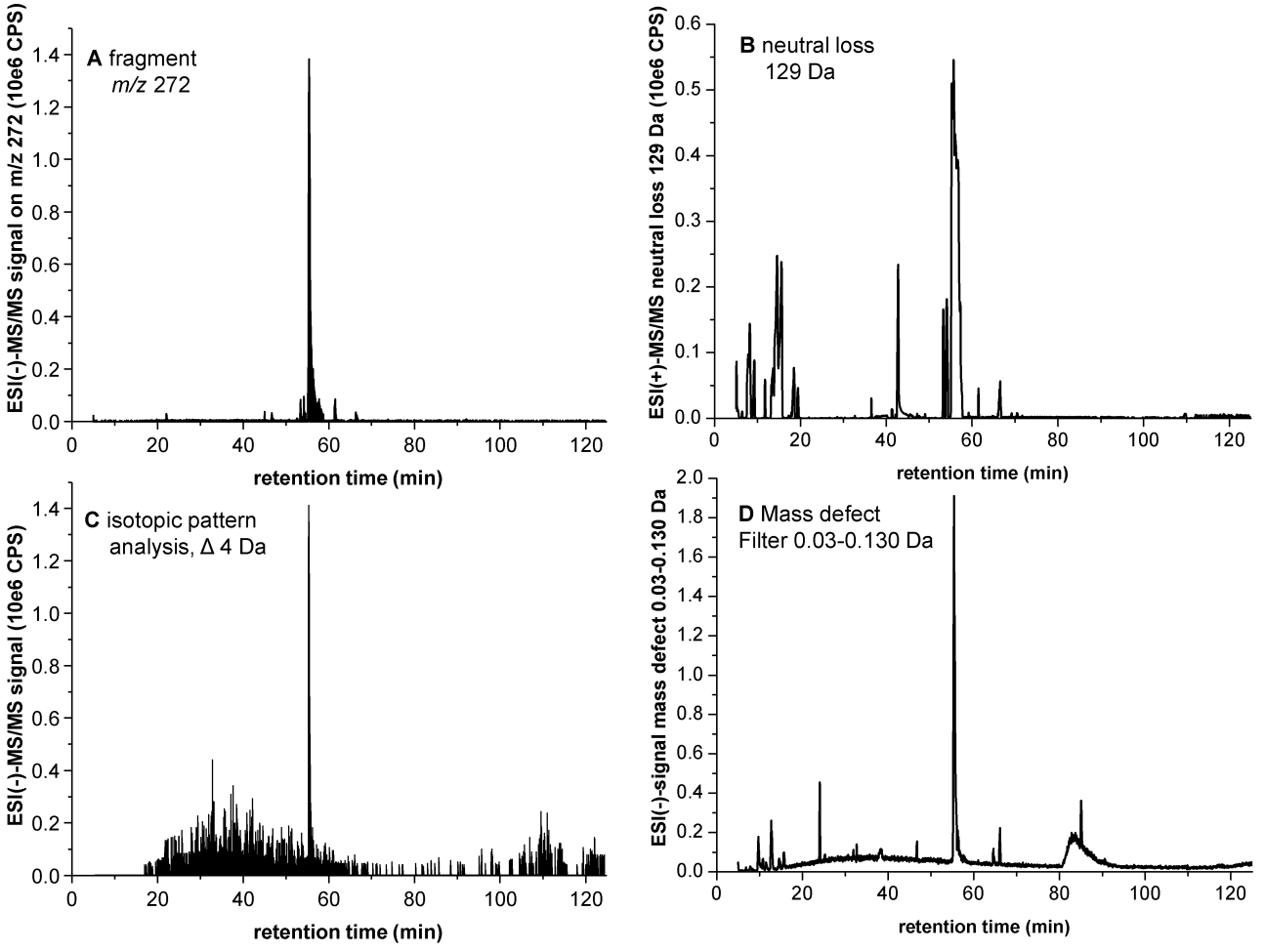
A fragment
m/z 272
ESI(-)-MS/MS signal on m/z 272 (10e6 CPS)
retention time (min)
B neutral loss
129 Da
ESI(+)-MS/MS neutral loss 129 Da (10e6 CPS)
retention time (min)
C isotopic pattern
analysis, Δ 4 Da
ESI(-)-MS/MS signal (10e6 CPS)
retention time (min)
D Mass defect
Filter 0.03-0.130 Da
ESI(-)-signal mass defect 0.03-0.130 Da
retention time (min)

Fig. 3

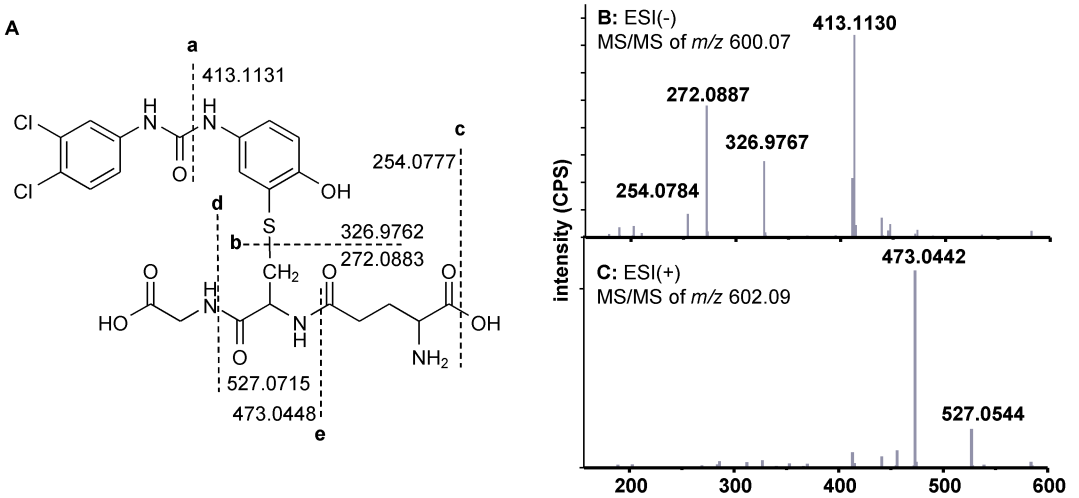
A
a
413.1131
Cl
Cl
H
N
O
H
N
c
254.0777
OH
d
S
b
326.9762
272.0883
CH2
O
O
HO
H
N
O
N
H
OH
NH2
527.0715
473.0448
e
B: ESI(-)
MS/MS of m/z 600.07
413.1130
272.0887
326.9767
254.0784
intensity (CPS)
C: ESI(+)
MS/MS of m/z 602.09
473.0442
527.0544
200
300
400
500
600

Fig. 4